Materials Transactions, Vol. 43, No. 8 (2002) pp. 1802 to 1807
Special Issue on Lead-Free Electronics Packaging

Mechanical Strength and Microstructure of BGA Joints Using Lead-Free Solders

Masataka Nishiura[1], Akihiro Nakayama[1], Sigeaki Sakatani[2,*], Yasuhiro Kohara[2,*], Keisuke Uenishi[2] and Kojiro F. Kobayashi[2]

[1]*Corporate Quality Administration Group, Matsushita Electronic Components Co., Ltd. Kadoma 571-8506, Japan*
[2]*Department of Manufacturing Science, Graduate School of Engineering, Osaka University Suita 565-0871, Japan*

Au–Ni plated Cu pads were reflow soldered by using lead free solder balls. The microstructure and strength of the as-reflowed solder joints were investigated. For solder joints using Cu-free Sn–Pb and Sn–Ag solder balls, a Ni_3Sn_4 reaction layer was formed on the boundary between solder and pads. On the other hand, a Cu–Sn based $(Cu, Ni)_6Sn_5$ reaction layer (η') was formed in solder joints using Cu-containing solder balls. The growth rate for an η' reaction layer during heat exposure at 423 K was much slower than that for a Ni_3Sn_4 reaction layer. This suppression of an η' reaction layer growth can be attributed to the fact that the Cu in solder balls was mostly removed during the formation of the η' layer. By ball shear test, cold bump pull and hot bump pull tests, mechanical properties of the obtained BGA joints were investigated. Fracture loads and crack propagation path changed by changing the mechanical tests, the BGA joints using Cu containing Sn–Ag–Cu solder or low P type Ni plating revealed better mechanical properties. We established the mismatch of the boundaries between reaction layers and the P-enriched Ni–P layer, which was caused by the chained voids formed due to the Kirkendall effect, led to low joint strength.

(Received February 27, 2002; Accepted May 28, 2002)

Keywords: *electrolessplating, ball grid array, lead free solder, intermetallic compound, shear strength, tensile strength, Phosphourus enriched Nickel-Phosphorus layer, chained voids, Kirkendall effect*

1. Introduction

Rapid developments in information technology have led to electronic equipment becoming smaller and gaining ever-higher performance. This has resulted in a growing need for increased numbers of input/output terminals and higher density mounting technology.[1)]

In LSI packaging, the application of ball grid array (BGA) packages to electronic equipment is becoming more common, since this type of package has the advantages of having higher input/output terminals and providing better electrical performance than more conventional packages, such as the pin through-hole or the quad flat package.[2)]

In BGA packaging, reflowed solder balls with a eutectic Sn–Pb composition have been used to connect the package electrically to the printed wiring board. For metallization of the Cu pads, Au pre-coated electroless Ni–P plating has been used to improve corrosion endurance and wettability.[3)] Since the formation and rapid growth of a brittle intermetallic layer during reflow soldering and its subsequent aging significantly degrade joint strength, the development of a good barrier technique to prevent excessive solder/pad interaction has been identified as a key challenge for microsoldering of electronics.[4)]

Recent environmental regulations outlawing Sn–Pb solder require the development of substitute Pb-free solders. After extensive studies, Sn–Ag eutectic alloy-based solders, which have superior mechanical properties, have come to the fore.[5–7)] Since most Pb-free solders have higher melting temperatures than conventional solder, the control of interfacial behavior, including the chemical reactions that take place between solder and pads, is now a focus of research interest.[8)]

*Graduate Student, Graduate School of Engineering, Osaka University, Suita 565-0871, Japan.

The present study was undertaken to investigate the interfacial reactions between different Sn–Ag-based Pb-free solders and Au pre-coated electroless Ni–P plated Cu pads under various reflow soldering conditions and to compare the results with those obtained for conventional Sn–Pb solder. Shear and tensile tests were performed to elucidate the mechanical properties of BGA joints, and the relation between joint microstructure and reliability is discussed.

2. Experimental Procedure

2.1 Samples

Substrates in which 5 µm Ni and 0.04 µm Au layers, respectively, were electroless-plated onto the Cu pads were used in this experiment. The Ni plating had three different P contents: about 5.4 mass% (low P-type), 7.2 mass% (middle P-type) and 10.2 mass% (high P-type). The compositions of solder balls used in this experiment were Sn–3.5 mass%Ag, Sn–3.5 mass%Ag–0.75 mass%Cu, Sn–2 mass%Ag–0.75 mass%Cu–3 mass%Bi and Sn–37 mass%Pb as reference; the diameter of the solder balls was 760 µm. A schematic view of solder joints is shown in Fig. 1. The solder balls were dipped into rosin flux and then were manually placed on the Cu pads. The solder balls were reflowed using an air reflow-soldering machine. The highest temperatures that the packages experienced were 513 K for in the case of Sn–Pb solder, and 523 K for the Sn–Ag, Sn–Ag–Cu, Sn–Ag–Cu–Bi solders.

2.2 Microstructure observation procedure

The cross-sections of samples were observed by scanning electron microscope (SEM) and the reaction layer was identified by wavelength dispersion X-ray (WDX) analysis to investigate the microstructure of the solder joints. In addition,

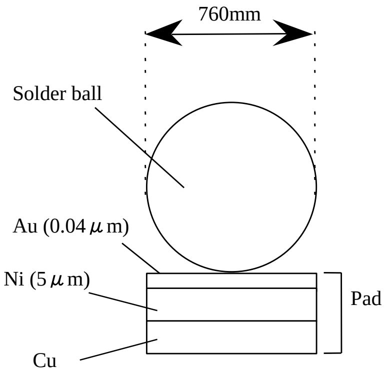

Fig. 1 Schematic view of solder joints.

to investigate the microstructure of solder joints in detail, secondary ion images (SIM images) generated by focused ion beam (FIB) of the cross-sections were observed to allow analysis.

2.3 Mechanical strength measurement procedure

The procedures for the mechanical strength measurements are shown in schematic form in Fig. 2. The shear strength of solder joints was measured using the ball shear test. The shear tool was set at a distance of 0.1 mm from the substrate. It was moved in parallel with the substrate at a speed of 0.2 mm/s. The tensile fracture load test comprised two types of test: the cold bump pull (CBP) test and the hot bump pull (HBP) test using the micro bond test apparatus (Dage Series 40000P and 2000PC). The cross-head speed was fixed to 0.3 mm/s for both tests. The mechanical tests were applied to ten samples each.

3. Results and Discussion

3.1 Microstructures of solder joints

Figure 3 shows the microstructures of the boundaries between solder and pads after reflow soldering and subsequent heating at 423 K for 500 h. The dispersion of needle-shaped Ag_3Sn in the Sn matrix was observed for the as-reflowed Sn–Ag solder joints, while a eutectic phase composed of Sn and Pb was observed for the as-reflowed Sn–Pb solder joints. By the addition of Cu, a Cu_6Sn_5 (η') phase newly appeared, although its volume fraction was smaller than for other phases. After heat exposure at 423 K, although coarsening of the Pb embedded in the Sn matrix was noticeable in the Sn–Pb solder, the Ag_3Sn phase changed its morphology to a more equiaxed shape.

On the boundaries between solder and pads, the Au plating layer completely disappeared from the boundaries just after reflow soldering, leaving a Ni layer exposed to the solder. On the boundaries between solder and pads, the formation of a reaction layer was confirmed for all solder joints. For the solder joints using Cu-free Sn–Pb and Sn–Ag solders, a Cu-free Ni and Sn-based reaction layer was formed. We have reported the formation of a metastable Ni (Au)–Sn compound with faster growth rate during heating at 423 K when the thickness of the Au plating exceeds about 1 µm.[9] In the present case, compositional analysis by WDX revealed the reaction layer to be an equilibrium phase of Ni_3Sn_4.

Furthermore, another newly layer was observed on the interface between the Ni_3Sn_4 layer and the Ni plating. This layer was identified by WDX analysis to be a Ni–P layer with a slightly higher P content than in the Ni plating. This compositional difference is caused by the diffusion of Ni from the Ni plating toward the solder to form a Ni_3Sn_4 layer.

For the solder joints using Cu containing Sn–Ag–Cu or Sn–Ag–Cu–Bi solders, a Cu and Sn-based η' reaction layer was formed on the solder and pad boundaries. A compositional analysis by WDX showed the η' layer to be composed of $(Cu_{1-x}, Ni_x)_6Sn_5$ by substitution of Ni atoms for a proportion of the Cu atoms. In this experiment, the η' layer was identified as $(Cu_{1-0.33}, Ni_{0.33})_6Sn_5$, but Kariya *et al*. have reported the η' phase to exist over a wide range, with Ni substituted for Cu by 50 at% or more.[10] Although Sn–Ag–Cu solder contains no more than 0.75 mass% of Cu, the addition of Cu to the solder was effective in changing the reaction layer from a Ni–Sn-based intermetallic compound to a Cu–Sn-based version. The Cu in Sn–Pb solder also behaves in the same way as that in Pb-free solder and forms a Cu–Sn intermetallic compound. Furthermore, the formation of a P-enriched Ni–P phase was observed, but it was thinner than that seen in solder joints using Cu-free solders.

Figure 4 shows the changes in the thickness of the reaction layers formed in the solder joints using Sn–Ag and Sn–Ag–Cu solders as a function of heat exposure time at 423 K. While the thickness of the η' reaction layer is slightly greater than a Ni_3Sn_4 layer for the as-reflowed solder joints, the growth rate of the Ni_3Sn_4 layer is much higher than that of the η' reaction layer. The growth rate of an η' reaction layer on the Cu/Sn boundaries is much higher than that of a Ni_3Sn_4 reaction layer on Ni/Sn boundaries.[11] In the present case, however, most of the Cu was consumed to form an η' reaction layer, and little Cu remains in the solder after reflow soldering, which slowed the growth rate of the η' reaction layer.

3.2 Mechanical properties of solder joints

3.2.1 Joint strengths resulting from different solder compositions

Figure 5 shows the average of the shear and tensile fracture loads of the as-reflowed solder joints using middle P-type Ni plating and various solders. Due to the different joint morphologies of each solder, these fracture loads do not always correspond to the joint strengths, but application of a range of different mechanical tests, we believe, is sufficient to indicate the overall joint strengths. The ball shear test results showed the joint strengths to be highest for Sn–Ag–Cu–Bi, followed in descending order by Sn–Ag–Cu, Sn–Ag and Sn–Pb. Notably, Sn–Ag–Cu–Bi solder showed about a 4 N higher joint strength than the other solders. For the CBP tensile test, the fracture loads were larger than those for the ball shear test; the fracture loads of the Sn–Ag solder were smaller than those of the other solders, but the fracture loads are unrelated with the solder compositions. For the HBP tensile test, the fracture loads for Sn–Ag–Cu solder were about 3.6 N larger than that for Sn–Pb solder, and that of Sn–Ag–Cu was three times greater than that for Sn–Ag solder.

Figure 6 shows the fracture paths of solder joints using middle P-type Ni plating and Sn–Pb and Sn–Ag–Cu solders after various mechanical tests. The results of the ball shear

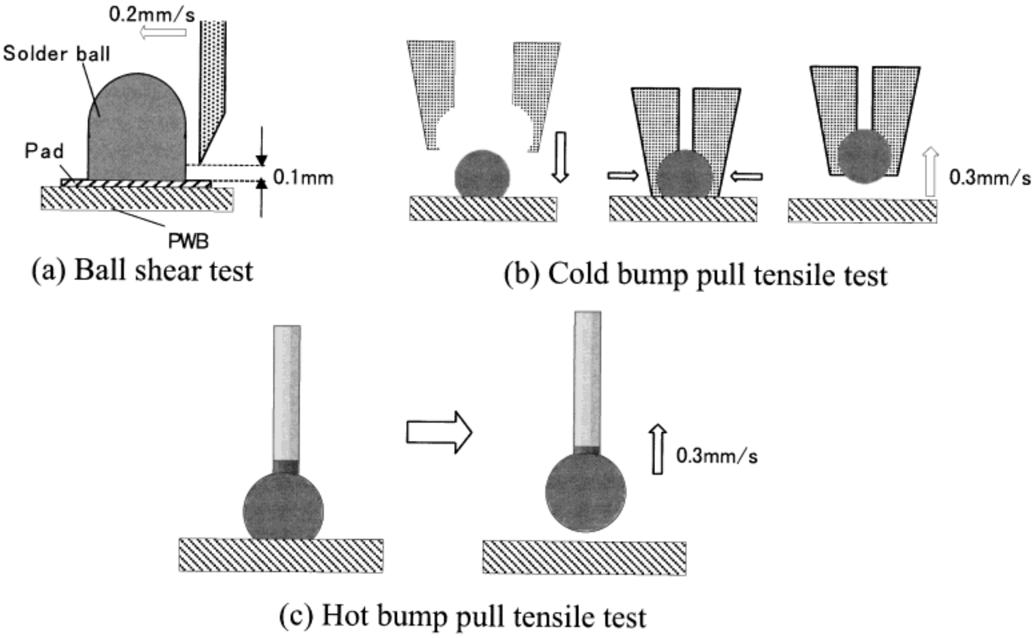

Fig. 2 Procedures for the mechanical strength measurements.

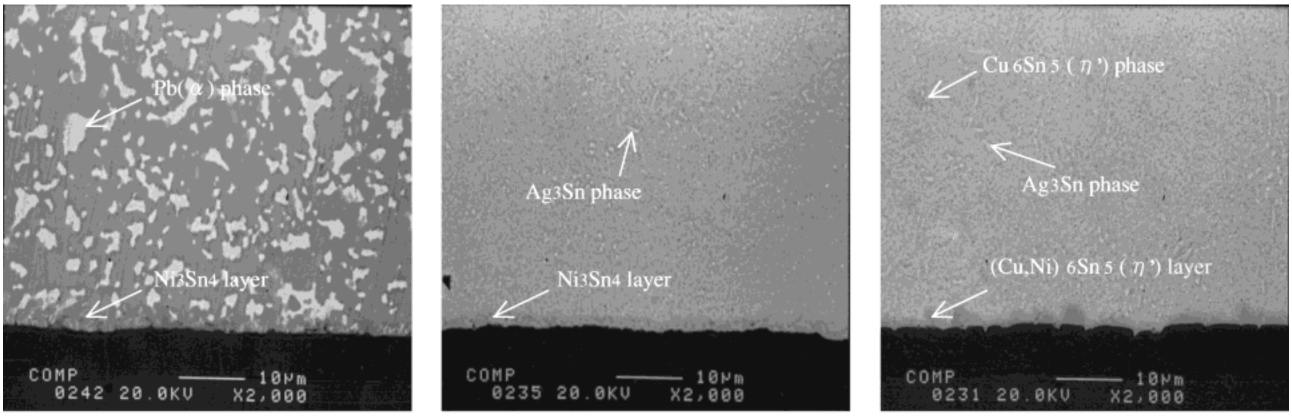

(a)Sn-37Pb (b)Sn-3.5Ag (c)Sn-3.5Ag-0.75Cu

Fig. 3 Microstructures of the boundaries between solder and pads after reflow soldering and subsequent heating at 423 K for 500 h.

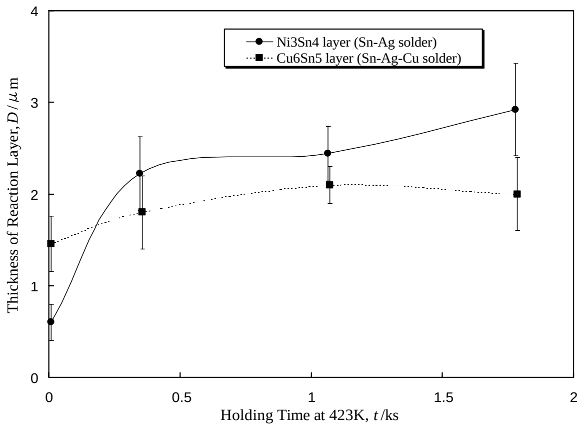

Fig. 4 Changes in the thickness of the reaction layers formed in the solder joints using Sn–Ag and Sn–Ag–Cu solders as a function of heat exposure time at 423 K.

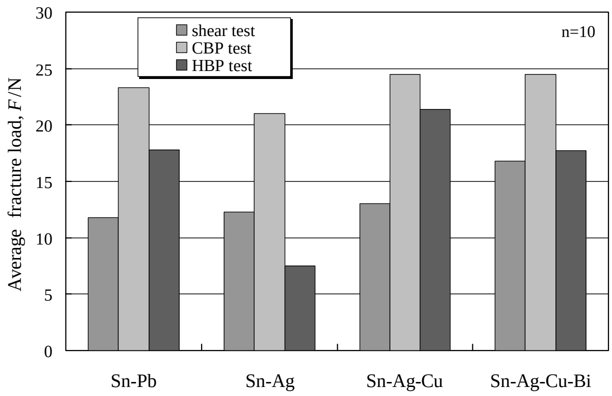

Fig. 5 Average of the shear and tensile fracture loads of the as-reflowed solder joints using middle P-type Ni plating and various solders.

test showed fractures to have occurred in most of the solder balls except a few samples using Sn–Ag–Cu–Bi solder. This explains the fact that the shear fracture loads depend on the strength of the solder balls. It is known that Sn–Ag based Pb-free solders have higher strength than Sn–Pb solder, and that the addition of Cu or Bi to these solders further increases their strength due to precipitation or solution hardening. The

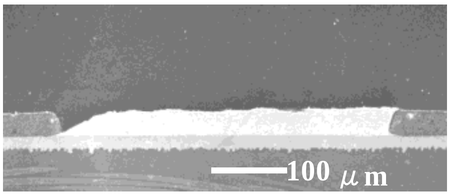

(a-1) Sn-Pb, shear

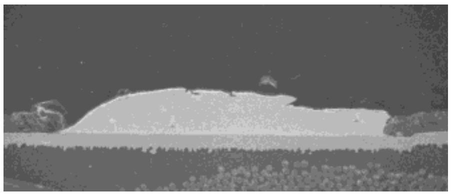

(b-1) Sn-Ag-Cu, shear

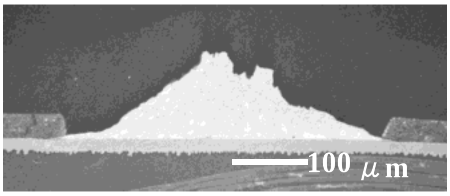

(a-2) Sn-Pb, CBP

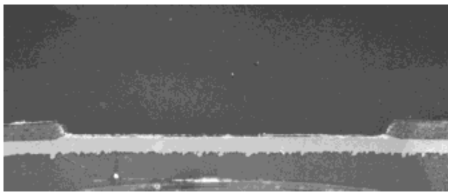

(b-2) Sn-Ag-Cu, CBP

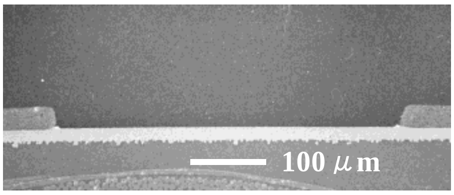

(a-3) Sn-Pb, HBP

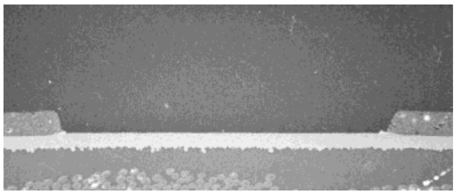

(b-3) Sn-Ag-Cu, HBP

Fig. 6 Fracture paths of solder joints using middle P-type Ni plating and Sn–Pb and Sn–Ag–Cu solders after various mechanical tests.

shear fracture loads obtained in this study correspond closely with the order of the strength of solders. The CBP tensile test showed that fractures occurred along the boundaries between reaction layers and Ni plating in addition to within the solder balls. In the HBP tensile test, all the samples fractured along the boundaries between the reaction layer and the Ni plating.

Since shear stress predominates in the ball shear tests, ductile destruction of the solder balls readily occurred. On the other hand, since tensile stress at 90° to the substrate predominates in the CBP and HBP tensile tests, the brittle destruction of the boundaries between reaction layers and Ni plating occurred more readily. However, in the case of fractures occurring in the solder ball during the CBP tensile test, the fracture propagated in the direction of 45° to the substrate. This means that tensile stress does not necessary act at 90° to the substrate.

3.2.2 Comparison of joint strength in relation to P content in Ni plating

Figure 7 shows the HBP fracture loads of the as-reflowed solder joints using Sn–Pb and Sn–Ag–Cu solders when the P content in the Ni plating is varied. The fracture loads decreased with increasing P content in the Ni plating. Notably for Sn–Ag–Cu solder, the fracture loads using low P-type Ni plating were about 22.49 N, those using middle P-type Ni plating were about 21.39 N, and those using high P-type Ni plating were about 19.53 N. The fracture loads using middle P-type Ni plating were about 95% larger and those using high P-type Ni plating were about 86% larger than those using low P-type Ni plating. For Sn–Pb solder, the fracture loads using low P-type Ni plating were about 20.63 N and those using middle P-type Ni plating were about 17.79 N. However, those using high P-type Ni plating were no more than 7.52 N. The fracture loads using middle P-type Ni plating were about 86% larger; those using high P-type Ni plating were only 36% of those using low P-type Ni plating.

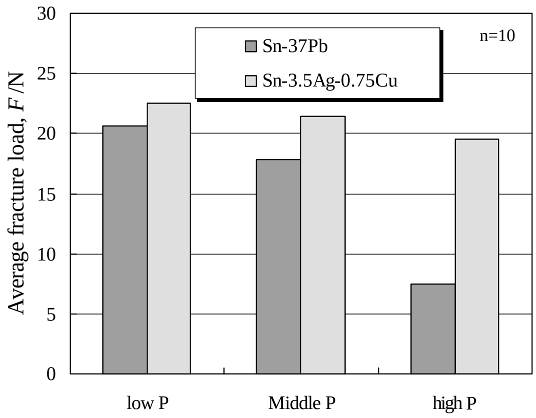

Fig. 7 HBP fracture loads of the as-reflowed solder joints using Sn–Pb and Sn–Ag–Cu solders when the P content in the Ni plating is varied.

3.3 Microstructure and joint strength

3.3.1 Relationship between solder composition and joint strength

Figure 8 shows SIM images of the cross-sections of solder joints using Sn–Pb, Sn–Ag and Sn–Ag–Cu solders and middle P-type Ni plating. The contrast between each reaction layer can be seen clearly by the difference of the etching rate for each layer using a focused gallium ion beam (FIB). For Cu-free Sn–Pb and Sn–Ag solder, a block-shaped Ni_3Sn_4 layer and a P-enriched Ni–P layer were formed on the boundaries between the solder and pads. The Ni_3Sn_4 layer in the

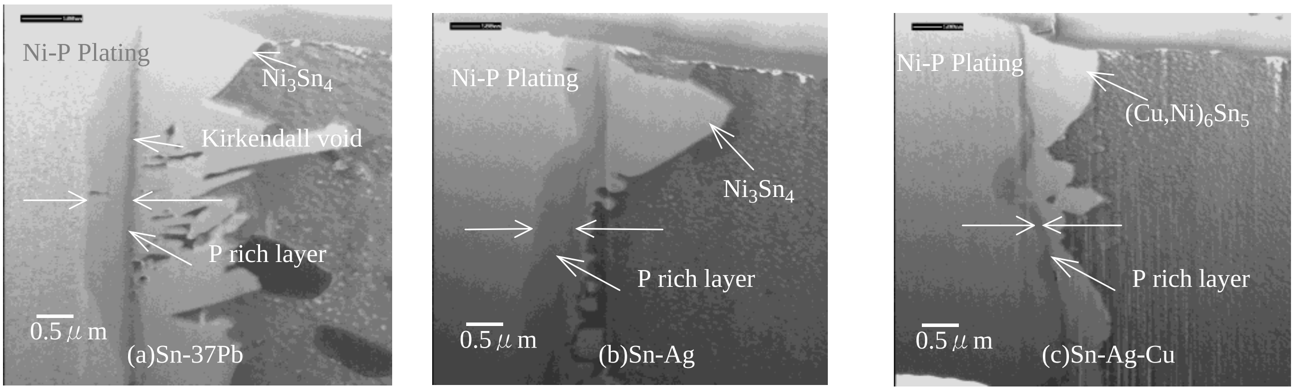

Fig. 8 SIM images of the cross-sections of solder joints using Sn–Pb, Sn–Ag and Sn–Ag–Cu solders and middle P-type Ni plating.

case of Sn–Ag solder was partially missing due to diffusion of Ni_3Sn_4 into the solder. The SIM images were then divided into seven equal parts and the thickness of each layer measured. The average thickness of the Ni_3Sn_4 layer was about 1.5 µm and 0.6 µm, respectively. On the other hand, the average thickness of a P-enriched Ni–P layer was about 540 nm and 590 nm, respectively. Furthermore, a dark gray layer and chained voids were observed on the boundaries between the Ni_3Sn_4 layer and the P-enriched Ni–P layer. The dark gray layer has been reported to be a Ni–Sn–P based compound layer.[10] It is assumed the chained voids were formed by the Kirkendall effect, due to the difference in the Ni diffusion coefficient for each layer, with the mismatch between the Ni_3Sn_4 layer and the P-enriched Ni–P layer due to the formation of the chained voids degrading the joint strength.

For the Cu-containing Sn–Ag–Cu solder, a block-shaped $(Cu, Ni)_6Sn_5$ layer and a P-enriched Ni–P layer were formed on the boundary between solder and pads. However, the average thickness of the $(Cu, Ni)_6Sn_5$ layer did not exceed 0.6 µm. This is why the Cu content was insufficient for formation of a $(Cu, Ni)_6Sn_5$ layer. The average thickness of the P-enriched Ni–P layer did not exceed 120 nm. Moreover, chained voids were formed in some areas between the $(Cu, Ni)_6Sn_5$ layer and the Ni–P–Sn layer as a result of Ni diffusion, so its volume is concluded to increase in proportion to the increase in average thickness of the P-enriched Ni–P layer. Figure 9 shows the relation between the fracture loads for the HBP tensile test and the thickness of the P-enriched Ni–P layer. The fracture loads decreased as the average thickness of the P-enriched Ni–P layer increased, but the fracture loads vs. the thickness of the P-enriched Ni–P layer did not show a linear relationship.

3.3.2 Relation between P content in Ni plating and joint strength

Figure 10 shows the SIM images of cross-sections of the solder joints using Sn–Pb solder with different P contents in the Ni plating. In the case of middle P-type Ni plating, a block-shaped Ni_3Sn_4 layer was formed, with an average thickness of 1.5 µm. For low middle P-type Ni plating, block-shaped Ni_3Sn_4 layer was formed in some areas, with an average thickness of 0.8 µm. For high P-type Ni plating, a Ni_3Sn_4 layer was formed with a mixture of a block and needle shapes, with an average thickness of 1.6 µm. Figure 11 shows the relation between the fracture loads measured using

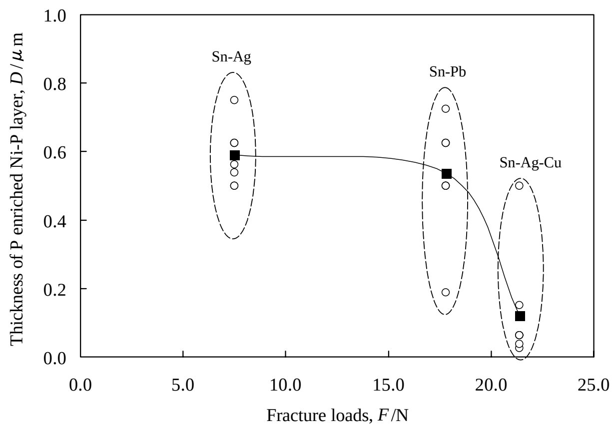

Fig. 9 Relation between the fracture loads for the HBP tensile test and the thickness of the P-enriched Ni–P layer.

the HBP tensile test and the thickness of the P-enriched Ni–P layer with different P contents in the Ni plating. As well as in the case of the solder compositions, the fracture loads decreased as the average thickness of the P-enriched Ni–P layer increased.

These results led to the following conclusions. The addition of Cu to solders changes the reaction layer from a Ni_3Sn_4 layer to a $(Cu, Ni)_6Sn_5$ layer, and the reduction of P content in the Ni plating delays the initiation and growth of a P-enriched Ni–P layer. These events lead to the suppression of chained voids, resulting in higher fracture loads for boundaries between solder and pads.

4. Conclusions

In this study, Sn–3.5 mass%Ag-based Pb-free solders were reflow soldered with Au/Ni electroless plated Cu pads as BGA packaging for electronics. The growth of solder joint microstructures and strength as a result of changing solder compositions and the P content in the Ni plating was investigated. The chief results obtained in this study are as follows.

(1) For solder joints using Cu-free Sn–Pb and Sn–Ag solder balls, a Ni_3Sn_4 reaction layer was formed on the boundary between solder and pads after reflow soldering and the subsequent heat storage at 423 K. On the other hand, a Cu–Sn based $(Cu, Ni)_6Sn_5$ reaction layer (η') was formed in solder joints using Cu-containing solder balls. The growth rate for

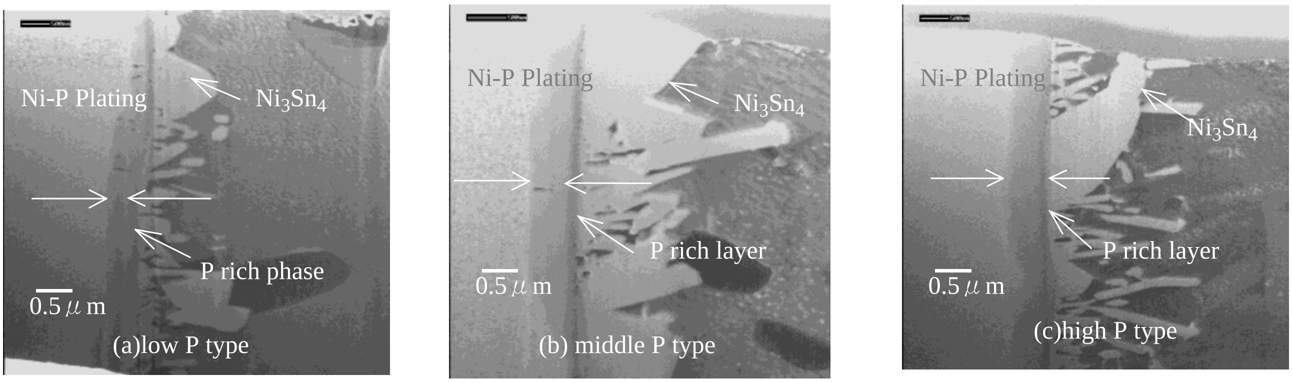

Fig. 10 SIM images of cross-sections of the solder joints using Sn–Pb solder with different P contents in the Ni plating.

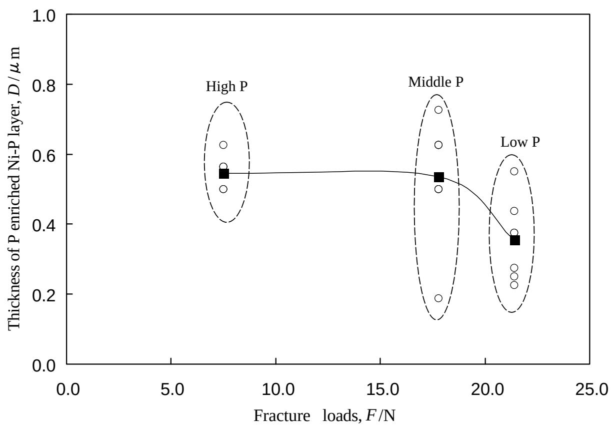

Fig. 11 Relation between the fracture loads measured using the HBP tensile test and the thickness of the P-enriched Ni–P layer with different P contents in the Ni plating.

an η' reaction layer during heat exposure at 423 K was much slower than that for a Ni_3Sn_4 reaction layer. This suppression of an η' reaction layer growth can be attributed to the fact that the Cu in solder balls was mostly removed during the formation of the η' layer and was present only at trace levels in the solder after reflow soldering.

(2) As for mechanical properties, especially for the HBP tensile test, the fracture loads of the solder joints using Cu containing Sn–Ag–Cu and Sn–Ag–Cu–Bi solders were larger than those using Cu-free Sn–Pb and Sn–Ag solders. Concerning the change in P content in the Ni plating, the fracture loads using low P-type Ni plating were greater than those using middle P-type and high P-type Ni plating. The mismatch of the boundaries between reaction layers and the P-enriched Ni–P layer was caused by the chained voids formed due to the Kirkendall effect, and this mismatch led to low joint strength. We have established that joint strength is closely related to the average thickness of the P-enriched Ni–P layer.

(3) A battery of mechanical tests revealed that BGA joints are more likely to fracture on the boundary between the reaction layer and the Ni plating. The HBP tensile test results showed that all of the solder joints fractured along this boundary.

REFERENCES

1) K. Suzuki and M. Nishiura: Proc. 30th Symposium on Reliability and Maintainability (JUSE, 2000) pp. 51–54.
2) E. Bradley and K. Banerji: IEEE Trans. Comp. Pkg. & Mfg. Technol. **B18** (1996) 320–331.
3) H. Simoyama, Y. Takase, J. Mizukosi and M. Nishiura: Proc. 7th Symposium on Microjoining and Assembly technologies for Electronics (JWS, 2001) pp. 237–240.
4) A. Hirose, T. Fujii, T. Imamura and K. F. Kobayashi: Mater. Trans. **42** (2001) 794–802.
5) M. Nishiura: Jpn J. of Electronics Packaging **3** (2000) 509–514.
6) M. Nishiura: Jpn J. of Electronics Packaging **3** (2000) 593–599.
7) S. Hirano, M. Nishiura and K. Tsutsui: Jpn. J. of Electronics Packaging **4** (2001) 41–46.
8) S. K. Kang, R. S. Rai and S. Purushothaman: Journal of Electronic Materials **25** (1996) 1113–1120.
9) S. Anhock, H. Oppermann, C. Kallmayer, R. Aschenbrenner, L. Thomas and H. Reichl: Proceedings of IEEE/CMPT Berlin International Electronics Manufacturing Technology Symposium (IEEE, 1998) pp. 156–165.
10) Y. Kariya, K. Nakamura, Y. Tanaka and M. Otsuka: Proc. 6th Symposium on Microjoining and Assembly technologies for Electronics (JWS, 2000) pp. 217–222.
11) P. Kay and C. A. Mackay: Trans. Inst. Met. Fin. **57** (1979) 169–176.